Missing p_{T} Reconstruction at ATLAS

Claire A. Lee
University of Johannesburg, South Africa
E-mail: claire.lee@cern.ch

Abstract. The missing transverse momentum ($E_{\mathrm{T}}^{\mathrm{miss}}$) in particle collider experiments is defined as the momentum imbalance in the plane transverse to the beam axis: the resultant of the negative vectorial sum of the momenta of all the particles that are involved in the *pp* collision of interest. A precise measurement of the $E_{\mathrm{T}}^{\mathrm{miss}}$ is essential for many physics studies at the LHC, such as Higgs boson searches and measurements, as well as searches beyond the Standard Model. The $E_{\mathrm{T}}^{\mathrm{miss}}$ measurement is constructed from the reconstructed and calibrated energy deposits inside the calorimeters, a method that has historically served experiments well, but one which is sensitive to fluctuations from noise and, in particular, additional unrelated collisions within the same event - an effect that is becoming more critical with the increasing luminosity of the LHC. A complementary method for measuring the missing transverse momentum is presented, in which track momenta are used in place of the calorimeter energy measurements, allowing the calculation to be made from particles originating solely from the collision vertex of interest. The reconstruction of this track-based missing transverse momentum, $p_{\mathrm{T}}^{\mathrm{miss}}$, and its performance in W and Z boson events, is described here.

1. Introduction

Missing transverse momentum ($E_{\mathrm{T}}^{\mathrm{miss}}$) is an essential part of many physics analyses at the LHC, including Higgs boson measurements and searches for beyond the Standard Model (BSM) signatures such as supersymmetric or hidden sector particles. After the *pp* scattering, most Standard Model (SM) particles produced leave traces inside the detector, however, SM neutrinos and some theorised BSM particles escape the detector without producing a signal. Since the momenta of the colliding protons in the transverse direction is essentially zero (in comparison to their boost along the beam direction), the presence of these particles can be inferred by a resultant momentum imbalance in the transverse plane. Ideally the $E_{\mathrm{T}}^{\mathrm{miss}}$ should be calculated using the final state particles from the hard *pp* interaction only (defined in ATLAS as the vertex with the highest scalar $\sum(p_T^{track})^2$), summing the momentum contributions from both charged and neutral particles over the full 4π solid angle. In practice, however, the detector phase space, reconstruction efficiencies, and the presence of additional "pileup" interactions from other *pp* scattering vertices in the same bunch crossing event, all affect the measurement.

2. The ATLAS Detector

The ATLAS detector [1] is a multipurpose system of particle detectors with nearly 4π solid angle coverage. It is composed of 3 core systems arranged in a barrel-plus-endcaps format. The inner detector (ID), covering the pseudorapidity range $|\eta| < 2.5$[1], consists of a 3-layered,

[1] In ATLAS, the positive x-axis is defined as pointing from the interaction point to the center of the LHC ring, the positive y-axis is defined as pointing upwards, and the positive z-axis corresponds to protons running

high granularity silicon pixel detector, followed by a silicon microstrip detector (SCT) with 8 layers, providing four two-dimensional measurement points per track. Additionally, a transition radiation tracker (TRT) adds extra tracking and electron identification ability within the $|\eta| < 2$ range. Surrounding the ID, a high granularity lead/liquid argon (LAr) sampling electromagnetic calorimeter covers the region $|\eta| < 3.2$ while a steel/scintillator-tile calorimeter provides hadronic coverage within $|\eta| < 1.7$. A Copper-LAr hadronic calorimeter is used in the end-cap region $1.5 < |\eta| < 3.2$. In the forward region, $3.1 < |\eta| < 4.9$, a copper-LAr electromagnetic calorimeter and a copper/tungsten-LAr hadronic calorimeter for a full energy measurement. Finally, the muon spectrometer (MS) surrounds the calorimeters, consisting of high-precision monitored drift tubes and cathode strip chambers for tracking in the barrel and endcaps respectively, providing accurate muon momentum measurements out to $|\eta| < 2.7$, as well as resistive plate chambers (barrel) and thin gap chambers (endcaps) for muon triggering in the region $|\eta| < 2.4$.

3. Missing Transverse Momentum Reconstruction at ATLAS

3.1. Calorimeter-based reconstruction

The primary detectors used for the $E_{\mathrm{T}}^{\mathrm{miss}}$ measurement in ATLAS are the electromagnetic and hadronic calorimeters, which are designed to provide excellent energy resolution at the LHC scale, and an optimised reconstruction and calibration procedure was developed by the collaboration for use during the LHC Run 1, described in detail in [2]. Calorimeter energy deposits are associated with high p_{T} objects, creating a term for each object type from their negative vectorial sum. Those not associated with high p_{T} objects are also taken into account, grouped into a "soft term" which includes contributions from both low p_{T} (<20 GeV) jets, and unassociated topoclusters. The $E_{\mathrm{T}}^{\mathrm{miss}}$ is then calculated as the vectorial sum of each of the terms. Another often-used quantity for parametrisation and event classification is the total transverse energy of the event, $\Sigma \mathrm{E_T}$, defined by the scalar sum of the same components. The advantage of this method is that it provides a complete measurement of all types of particles involved in the pp interaction. However, energy contributions from pileup vertices can provide sources of "fake" $E_{\mathrm{T}}^{\mathrm{miss}}$ and decrease the resolution significantly. To combat this, the precise tracking and vertexing ability of the ID is taken advantage of.

3.2. Track-based reconstruction

Similar to the calorimeter-based method, individual terms for electrons, jets, and muons are formed, except that here the terms instead use the momenta of the ID tracks associated with the leptons and jets. In place of the calorimeter cluster-based "soft term", only tracks originating from the signal vertex of interest that have not already been included in the lepton or jet terms are used, forming a "track soft term". The nominal $p_{\mathrm{T}}^{\mathrm{miss}}$ is then:

$$\mathbf{p}_{x,y}^{\mathrm{miss,nominal}} = -\left(\sum_{electron\ tracks} \mathbf{p}_{x,y} + \sum_{muon\ tracks} \mathbf{p}_{x,y} + \sum_{jet\ tracks} \mathbf{p}_{x,y} + \sum_{soft\ tracks} \mathbf{p}_{x,y} \right) \quad (1)$$

with

$$\mathbf{p}_{\mathrm{T}}^{\mathrm{miss,nominal}} = \sqrt{\left(\mathbf{p}_{x}^{\mathrm{miss,nominal}}\right)^2 + \left(\mathbf{p}_{y}^{\mathrm{miss,nominal}}\right)^2} \quad (2)$$

with the advantage that it provides a measurement that is almost completely decoupled from the $E_{\mathrm{T}}^{\mathrm{miss}}$, and relates to the signal vertex only. The disadvantage of this measurement, of course, is

anticlockwise. The polar angle θ is measured from the beam axis (z-axis), the azimuthal angle ϕ is measured in the transverse (xy)-plane, and the pseudorapidity is defined by $\eta = -\log(\tan(\theta/2))$.

that it is restricted only to charged particles, as well as by the smaller acceptance of the ID. For certain event topologies the effect is minor, but in events with jets where a significant fraction of the jet momentum comes from neutral particles, or where high p_{T} objects are boosted in the forward directions, missing their momenta leads to a significant decrease in the resolution. A second, object-corrected $p_{\mathrm{T}}^{\mathrm{miss}}$ is therefore defined, where the terms containing the associated tracks for each high p_{T} object are replaced by their reconstructed and fully calibrated momentum counterpart, while retaining the track soft term. In this way, we are able to account for the full p_{T} of jets in both the central and forward regions, electron energies without any radiation losses, and a more accurate high p_{T} muon momentum reconstruction, while maintaining the relation to the signal vertex.

3.3. Track and high p_{T} object selection criteria

All tracks included in the $p_{\mathrm{T}}^{\mathrm{miss}}$ track soft term reconstruction must satisfy the following criteria:

- $p_T > 500$ MeV
- $|\eta| < 2.5$
- At least 1 pixel detector hit
- At least 6 SCT hits
- Transverse impact parameter with respect to the primary vertex $|d_0| < 1.5$ mm
- Longitudinal impact parameters with respect to the primary vertex $|z_0 \times \sin(\theta)| < 1.5$ mm.

The selections ensure that the tracks have enough points for an accurate p_{T} measurement, are associated to the signal vertex, and are within the ID acceptance. Additional selection criteria for specialised cases are also performed, such as removing unwanted tracks around high p_{T} electrons (due to misreconstruction) and badly measured tracks in dense, high p_{T} jets. General tracks with extremely high momenta are also checked against corresponding calorimeter cluster deposits to reduce the number of misreconstructed tracks.

Electrons, muons and jets are selected to complement the method used for the $E_{\mathrm{T}}^{\mathrm{miss}}$. Good quality muons with $p_{\mathrm{T}} > 6$ GeV reconstructed from combined ID and MS tracks, and isolated electrons with $p_{\mathrm{T}} > 10$ GeV are considered for their respective terms. The tracks associated with the selected leptons are obtained using the stored track-to-object information in the data. Jets are reconstructed with the anti-kt algorithm [3] using a distance parameter of R = 0.4, with corrections for pileup at the topocluster level, and subsequent calibrations using the LCW+JES scheme [4, 5]. Jets are selected if their calibrated p_{T} is greater than 25 GeV in the central region ($|\eta| < 2.5$), or 30 GeV in the forward region ($2.5 < |\eta| < 4.4$), and they do not overlap with any of the selected electrons. In addition, a cut on the jet vertex fraction (JVF [6]) of JVF > 0.50 is required for jets with calibrated $p_T < 50$ GeV and $|\eta| < 2.4$, which helps to reduce the selection of pileup jets in the central region. The jet tracks are obtained using the ghost association algorithm [7], and are also required to pass the high quality track requirements described above.

4. $p_{\mathrm{T}}^{\mathrm{miss}}$ Performance in $\mathrm{W} \to \ell\nu$ and $\mathrm{Z} \to \ell\ell$ events

W and Z boson production is relatively abundant at the LHC, and their leptonic decays provide clear experimental signatures with well understood topologies that make them ideal events for measuring the performance of our detector and reconstruction algorithms. The absence of real $E_{\mathrm{T}}^{\mathrm{miss}}$ in $\mathrm{Z} \to \ell\ell$ events allows us to measure the intrinsic resolution and performance of the $p_{\mathrm{T}}^{\mathrm{miss}}$ that results mainly from detector response and object reconstruction efficiencies, whereas in $\mathrm{W} \to \ell\nu$ events the neutrino provides a good metric against which to measure the $p_{\mathrm{T}}^{\mathrm{miss}}$ scale and direction.

4.1. Datasets used and $\mathrm{W} \to \ell\nu$ *and* $\mathrm{Z} \to \ell\ell$ *event selection*

The dataset used for this study was recorded by the ATLAS detector in the 2012 run at a $\sqrt{s} = 8$ TeV centre of mass energy while all detector subsystems were operating efficiently, with a total integrated luminosity of 20.3 fb^{-1}. Events were required to pass standard detector quality assessment criteria and fire a single or dilepton trigger to be considered. For good vertex reconstruction, the primary vertex is required to have at least three associated reconstructed tracks with $p_T > 400$ MeV each. For $\mathrm{Z} \to \ell\ell$ events, events were selected if they contained exactly two same flavour, opposite charge good quality leptons with $p_{\mathrm{T}} > 25$ GeV, and a combined invariant mass of between 66 and 116 GeV. For $\mathrm{W} \to \ell\nu$ events, exactly one good quality lepton with $p_{\mathrm{T}} > 25$ GeV, and an $E_{\mathrm{T}}^{\mathrm{miss}} > 30$ GeV was required. Furthermore, the invariant mass of the lepton-$E_{\mathrm{T}}^{\mathrm{miss}}$ system was calculated and required to be at least 50 GeV.

Monte Carlo samples of $\mathrm{Z} \to \ell\ell$ and $\mathrm{W} \to \ell\nu$ + n jets ($\ell = e, \mu, \tau$) production were generated using ALPGEN [8] interfaced to Jimmy [9], with up to 6 partons in the final state. Additional background samples of $t\bar{t}$ events were produced with the MC@NLO event generator [10], and WW, WZ, and ZZ diboson samples were produced using HERWIG [11].

4.2. $p_{\mathrm{T}}^{\mathrm{miss}}$ *data vs simulation comparisons*

Data versus Monte Carlo simulation comparisons for the nominal and object-corrected $p_{\mathrm{T}}^{\mathrm{miss}}$ in inclusive $\mathrm{Z} \to ee$ events are shown in figure 1, showing signal and relevant background Monte Carlo distributions ordered by their (weighted) integral so that all background distributions are visible, as well as the data-to-background ratio in the panel below. The error on the ratio points is calculated from the statistical uncertainty of the observed data, and the grey error bands show the total uncertainty from the expected background. A good comparison is obtained between the data and the simulated backgrounds for both the nominal and object-corrected $p_{\mathrm{T}}^{\mathrm{miss}}$, particularly in the peaks, but with some discrepancy in the tails where statistics are low. Some background contribution from QCD processes in these events is also expected, particularly in the low $p_{\mathrm{T}}^{\mathrm{miss}}$ region. These processes are not well simulated and therefore are not included in the background set, giving rise to the discrepancy in the data/background ratio in this region. A peak close to zero is seen as expected for events with no real $E_{\mathrm{T}}^{\mathrm{miss}}$. The broader peak in the nominal distribution is a result of mismeasured electron track p_{T} due to Bremsstrahlung, an effect which is mitigated in the object-corrected case. Also noticeable is the reduced tail in the object-corrected distribution, as the momenta of any jets in the event is fully taken into account. Similar distributions are obtained for the $\mathrm{Z} \to \mu\mu$ channel, though the corresponding nominal distribution does not, of course, have the broader peak.

4.3. $p_{\mathrm{T}}^{\mathrm{miss}}$ *resolution and scale*

The resolution of the $p_{\mathrm{T}}^{\mathrm{miss}}$ is defined as the width of the peak in the x and y component distributions, and is sensitive to both detector and reconstruction efficiencies, as well as external factors like the presence of pileup. The resolution of the nominal and object-corrected $p_{\mathrm{T}}^{\mathrm{miss}}$ is flat as a function of the number of reconstructed primary vertices in the event (N_{pv}), and the values for $\mathrm{W} \to \ell\nu$ and $\mathrm{Z} \to \ell\ell$ events are shown in table 1. The resolution can also be parameterised as a function of the event activity, using:

$$y = k\sqrt{\sum E_T} + c \tag{3}$$

where k and c are constants obtained from a fit of the above function. The resolution for $\mathrm{Z} \to ee$ and $\mathrm{W} \to e\nu$ events as a function of $\sqrt{\sum E_T}$ is shown in figure 2 (a), and the k-values obtained from the fits to the data are also given in table 1 (c is ideally 0 and, in these fits, effectively 0, and so is not shown).

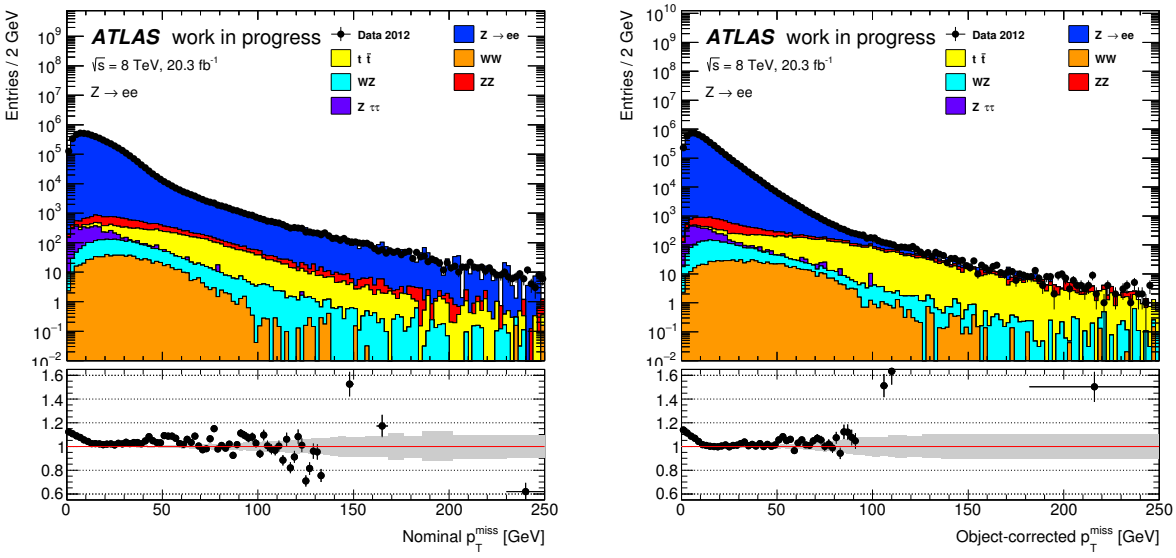

(a) (b)

Figure 1: Data-to-Monte Carlo comparisons of the nominal (a) and object-corrected (b) $p_{\mathrm{T}}^{\mathrm{miss}}$in $\mathrm{Z} \to ee$ events.

Table 1: $p_{\mathrm{T}}^{\mathrm{miss}}$ resolution and $\Sigma \mathrm{E_T}$ fit values

	$\mathrm{Z} \to ee$ Data	$\mathrm{Z} \to ee$ MC	$\mathrm{W} \to e\nu$ MC
Nominal $p_{\mathrm{T}}^{\mathrm{miss}}$ resolution vs N_{pv}[GeV]	10.49	10.33	9.63
Object-corrected $p_{\mathrm{T}}^{\mathrm{miss}}$ resolution vs N_{pv}[GeV]	7.54	7.23	7.15
Nominal $p_{\mathrm{T}}^{\mathrm{miss}}$ fit to ΣE_T (k)	0.28	0.26	0.21
Object-corrected $p_{\mathrm{T}}^{\mathrm{miss}}$ fit to ΣE_T (k)	0.28	0.26	0.24
	$\mathrm{Z} \to \mu\mu$ Data	$\mathrm{Z} \to \mu\mu$ MC	$\mathrm{W} \to \mu\nu$ MC
Nominal $p_{\mathrm{T}}^{\mathrm{miss}}$ resolution vs N_{pv}[GeV]	7.63	7.40	7.12
Object-corrected $p_{\mathrm{T}}^{\mathrm{miss}}$ resolution vs N_{pv}[GeV]	7.51	7.28	7.02
Nominal $p_{\mathrm{T}}^{\mathrm{miss}}$ fit to ΣE_T (k)	0.27	0.26	0.20
Object-corrected $p_{\mathrm{T}}^{\mathrm{miss}}$ fit to ΣE_T (k)	0.29	0.28	0.22

In events with real $E_{\mathrm{T}}^{\mathrm{miss}}$ the scale of the measurement is also important. The linearity of the $p_{\mathrm{T}}^{\mathrm{miss}}$ with respect to the true $E_{\mathrm{T}}^{\mathrm{miss}}$ in an event is defined as the mean of the ratio:

$$\text{Linearity} = \langle \frac{p_{\mathrm{T}}^{\mathrm{miss}} - E_{\mathrm{T}}^{\mathrm{miss,truth}}}{E_{\mathrm{T}}^{\mathrm{miss,truth}}} \rangle \tag{4}$$

which gives an expected value of zero if the $p_{\mathrm{T}}^{\mathrm{miss}}$ is reconstructed at the correct scale. The linearity distributions for the nominal and object-corrected $p_{\mathrm{T}}^{\mathrm{miss}}$ is shown in figure 2 (b) for both $\mathrm{W} \to e\nu$ and $\mathrm{W} \to \mu\nu$ events. A positive bias is visible in the region of very low true $E_{\mathrm{T}}^{\mathrm{miss}}$, owing to the finite resolution of the $p_{\mathrm{T}}^{\mathrm{miss}}$ and the domination of contributions in the soft track term. At larger values of true $E_{\mathrm{T}}^{\mathrm{miss}}$, the bias is within 5% for the object-corrected $p_{\mathrm{T}}^{\mathrm{miss}}$, with a larger negative bias in the nominal $p_{\mathrm{T}}^{\mathrm{miss}}$ as expected due to jets. Differences in the linearity

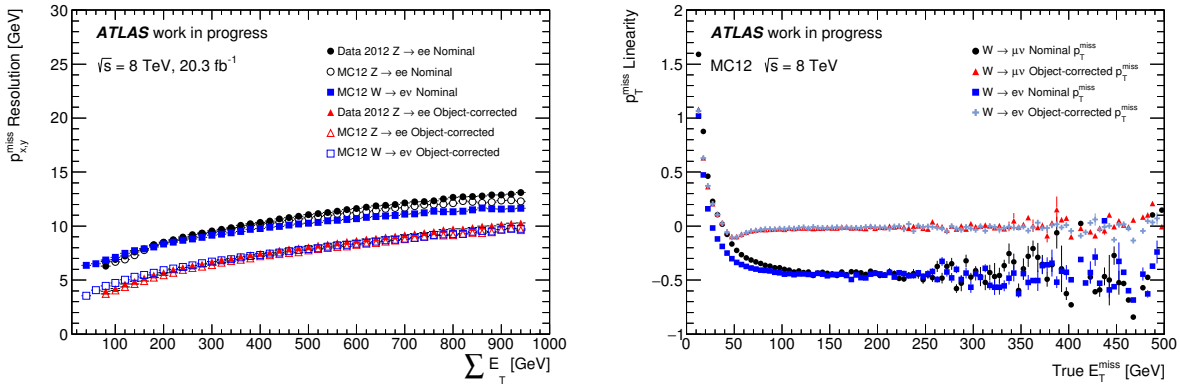

(a) (b)

Figure 2: Resolution of the x and y components of the nominal and object-corrected $p_{\mathrm{T}}^{\mathrm{miss}}$ for $\mathrm{Z} \to ee$ and $\mathrm{W} \to e\nu$ events as a function of the scalar sum of the total transverse energy in the calorimeter. (b) Nominal and object-corrected $p_{\mathrm{T}}^{\mathrm{miss}}$ linearity with respect to the true $E_{\mathrm{T}}^{\mathrm{miss}}$ in $\mathrm{W} \to e\nu$ and $\mathrm{W} \to \mu\nu$ events

for the electron and muon channels can also be seen for the nominal $p_{\mathrm{T}}^{\mathrm{miss}}$, where the electron momentum loss shows again in a worsening of the bias (though the effect at higher values of true $E_{\mathrm{T}}^{\mathrm{miss}}$ is diminished).

5. Conclusions

The measurement of missing energy is an important contribution to a number of interesting physics analyses. The ATLAS calorimeter provides excellent energy resolution but is highly sensitive to pileup. A track-based $p_{\mathrm{T}}^{\mathrm{miss}}$ calculation can be made using the momentum of tracks inside the ATLAS ID, taking advantage of the fact that ID tracks can be selected from a single primary vertex, allowing for much greater pileup stability than the calorimeter-based measurement. The performance of the nominal $p_{\mathrm{T}}^{\mathrm{miss}}$ degrades in events with jets owing to the larger fraction of neutrals and the fiducial coverage, and in events with electrons due to Bremsstrahlung. This is improved by using the fully reconstructed object term instead of the associated tracks for high p_{T} objects. Both versions of the $p_{\mathrm{T}}^{\mathrm{miss}}$ show good performance for a number of Run 1 event topologies, with Monte Carlo simulations that describe the data well, excellent resolution stability with pileup, and a good measurement of the scale of the event.

References

[1] Aad G *et al.* (ATLAS Collaboration) 2008 *JINST* **3** S08003
[2] Aad G *et al.* (ATLAS Collaboration) 2013 *ATLAS-CONF-2013-082*
[3] Cacciari M, Salam G P and Soyez G 2008 *JHEP* **0804** 063 (*Preprint* `0802.1189`)
[4] Aad G *et al.* (ATLAS Collaboration) 2013 *Eur.Phys.J.* **C73** 2304 (*Preprint* `1112.6426`)
[5] Aad G *et al.* (ATLAS Collaboration) 2014 (*Preprint* `1406.0076`)
[6] Aad G *et al.* (ATLAS Collaboration) 2009 (*Preprint* `0901.0512`)
[7] Cacciari M and Salam G P 2008 *Phys.Lett.* **B659** 119–126 (*Preprint* `0707.1378`)
[8] Mangano M L, Moretti M, Piccinini F, Pittau R and Polosa A D 2003 *JHEP* **0307** 001 (*Preprint* `hep-ph/0206293`)
[9] Butterworth J, Forshaw J R and Seymour M 1996 *Z.Phys.* **C72** 637–646 (*Preprint* `hep-ph/9601371`)
[10] Frixione S and Webber B R 2002 *JHEP* **0206** 029 (*Preprint* `hep-ph/0204244`)
[11] Corcella G, Knowles I, Marchesini G, Moretti S, Odagiri K *et al.* 2001 *JHEP* **0101** 010 (*Preprint* `hep-ph/0011363`)